Eur. J. Mineral.
2000, 12, 923-934

TEM study of the mechanism of transformation of detrital kaolinite and muscovite to illite/smectite in sediments of the Salton Sea Geothermal Field

GIOVANNA GIORGETTI[1], M. PILAR MATA[2] and DONALD R. PEACOR[3]

[1]Department of Earth Sciences, University of Siena, Via Laterina, 8, 53100 Siena, Italy
e-mail (corresponding author): giorgettig@unisi.it
[2]Department of Geology, University of Cádiz, Pol. Rio San Pedro, 11510 Puerto Real (Cádiz), Spain
[3]Department of Geological Sciences, The University of Michigan, Ann Arbor, MI 48109-1063, USA

Abstract: The reaction by which kaolinite transforms to I-S has been studied by SEM and TEM using core samples from the Salton Sea Scientific Drilling Project. Kaolinite is abundant from the surface to a depth of ~300 m (~115 °C), decreasing in abundance and becoming undetectable at a depth of ~500 m (~160 °C), with a concomitant increase in abundance of I-S. In a 256-m deep sample, kaolinite occurs as large (~100 μm) detrital grains, in the fine-grained (< 1 μm) matrix, and as packets forming stacks in detrital biotite and muscovite. In sharp contrast, no kaolinite was detected in the sample from a depth of 477 m but illite and minor I-S occur in the matrix. Authigenic chlorite occurs as subhedral crystals in the matrix with subparallel illite crystals, and as muscovite-chlorite stacks. I-S occurs in three ways: (1) Interlayered within kaolinite as a few, curved layers with 10- and 20-Å periodicities with the characteristics of collapsed, dehydrated I-S. Along-layer transitions with change in (00l) d-value from 7 to 10 Å occur. (2) As coalescent, randomly oriented packets filling pore space in the matrix. (3) Interlayered with detrital muscovite.

These observations show that R1 I-S in Salton Sea-area sediments forms primarily through alteration of kaolinite and muscovite of detrital origin over a temperature interval of ~100 to < 200 °C, with I-S serving as a precursor to illite. Reaction occurs both by direct layer-by-layer replacement of kaolinite and muscovite, and by dissolution, ion transport and crystallization in pore space. Both processes involve dissolution and crystallization, with only the scale of transport varying from that of along-layer interfaces to the dimensions of pore space. The pH value and activity of K^+ in the hydrothermal brines play important roles in the alteration process and control the simultaneous transformation of both kaolinite and muscovite to I-S.

Key-words: kaolinite, muscovite, TEM, transformation, I-S.

Introduction

Kaolinite is a common detrital mineral in sediments and is also widely recorded in diagenetic sequences where it is authigenic in origin. Where extended sediment sequences have been studied, kaolinite has frequently been found to react to other phases with increasing grade. For example, powder X-ray diffraction (XRD) studies have documented transitions involving kaolinite that occur during diagenesis and low-grade metamorphism (Muffler & White, 1969; Hower *et al.*, 1976; Boles & Franks, 1979; Ahn & Peacor, 1985; Primmer, 1985; Frey, 1987; Yau *et al.*, 1988; Arostegui *et al.*, 1991; Nieto *et al.*, 1996).

Boles & Franks (1979) studied Wilcox sandstone sequences over a range of depth from 975 to 4650 m, corresponding to a temperature range of 55 to 210 °C. They showed that kaolinite could no longer be detected at the same depths where chlorite was found, over the temperature interval

0935-1221/2000/0012-0923 $ 3.00

from 150 to 200 °C. Similarly, in the Paleozoic clastic sequence from the Variscan fold/thrust belt, the amount of diagenetic kaolinite decreases as chlorite content increases at temperatures below 200 °C (Primmer, 1985). Those authors hypothesized that kaolinite reacts with Fe and Mg released during the smectite-to-illite transformation to form chlorite with high Al contents. Other authors (Frey, 1987; Arostegui *et al.*, 1991; Ruiz-Cruz & Andreo, 1996) inferred that the proportion of kaolinite decreases during diagenesis and low-grade metamorphism either through the discontinuous reaction kaolinite + quart = pyrophyllite + H_2O or through a reaction in which I-S forms.

A particularly well-defined transition involving the loss of kaolinite occurs in sediments of the Salton Sea Geothermal Field (SSGF), for which several studies have investigated mineralogical changes as a function of depth and increasing temperature (*e.g.*, McDowell & Elders, 1980; McDowell & Paces, 1985; McDowell, 1986; Yau *et al.*, 1987a, 1988; Cho *et al.*, 1988; Shearer *et al.*, 1988). XRD data revealed that kaolinite is abundant in sediments from the surface to a depth of ~300 m (T ≈ 115 °C). However, with further increase in depth it decreases in abundance as the proportions of I-S, illite and chlorite increase, until it can no longer be detected at a depth of ~500 m (T~160 °C). The SSGF occurs in an environment of active rifting and high geothermal gradient, resulting in convecting hydrothermal fluids that give rise to continuing "hydrothermal metamophism" of sediments. The Salton Sea Scientific Drilling Project (SSSDP) successfully drilled numerous bore holes to a depth > 3200 m and temperatures > 350 °C. Hence the SSSDP samples provide a unique opportunity for a comprehensive study of an actively evolving hydrothermal-metamorphic system.

Despite the many studies which have defined prograde reactions in which kaolinite is a reactant, little is known about the reaction mechanisms and textures, compositions, and structures of the minerals involved. Such relations can generally only be characterized by transmission electron microscopy (TEM), but no such TEM studies have been performed on reactions involving kaolinite in the zone of diagenesis. We have carried out a scanning electron microscopy (SEM) and TEM study of the Salton Sea sediments to characterize the textural and structural characteristics of kaolinite and other reactants and products, and determine the mechanism by which kaolinite is lost during low-grade metamorphism.

Geological setting

The SSGF is located near the center of the Salton Trough (Figure 1 in Helgeson, 1968; Figure 1 in McDowell & Elders, 1980), at the southern end of the San Andreas fault system. It is a site of active rifting and frequent seismic activity. Fluvio-deltaic sediments derived from the Colorado River system and evaporitic and lacustrine sediments have been deposited in the Salton Trough since the Pliocene (Merriam & Bandy, 1965; Muffler & Doe, 1968). Elevated geothermal gradients are associated with rhyolitic volcanism, and the geothermal system has been active for 16000 years based on whole-rock K/Ar age determinations (Kistler & Obradovich in Muffler & White, 1969). The SSGF is characterized by anomalously concentrated NaCl-$CaCl_2$-KCl brines with a relatively low pH (Helgeson, 1967, 1968).

The many wells drilled by the SSSDP (for a review see Younker *et al.*, 1982) revealed that the terrigenous sediments have undergone a complex history of active metamorphism and hydrothermal alteration in response to recent volcanism and active faulting. Mineralogical, chemical and textural changes associated with metamorphism have been investigated by many authors (Helgeson, 1968; McDowell & Elders, 1980; Yau *et al.*, 1987b, 1988; Cho *et al.*, 1988; Shearer *et al.*, 1988). Based on the appearance of authigenic minerals, four metamorphic zones have been distinguished: 1) The dolomite-ankerite zone at depths <439 m, which corresponds to temperatures of ~190 °C. Dolomite/ankerite occur with I-S, calcite, hematite, sphene, and quartz. 2) The calcite-chlorite zone, from 439 to 1135 m (190–325 °C), in which chlorite, illite, I-S, sphene, calcite, albite, K-feldspar, pyrite, and quartz occur. 3) The biotite zone, from 1135 to 2120 m (325–360 °C), in which biotite, quartz, epidote, K-feldspar, albite, talc, pyrite ±actinolite occur with traces of phengite, chlorite, and vermiculite. 4) The garnet zone, at <2115 m (temperatures > 360 °C), in which andradite garnet occurs with biotite, quartz, albite, epidote, actinolite, pyrite and sphene. As the biotite "isograd" is approached, the grain morphologies typical of detrital grains become modified and the sandstones are progressively transformed into hornfelsic rocks.

Samples and analytical techniques

Samples used in this study came from the California State 2-14 well, for which SEM-BSE (back-scattered electron) and XRD analyses (Cho *et al.*, 1988; Shearer *et al.*, 1988) have documented an increase in metamorphic grade from the chlorite-calcite zone up to the lower amphibolite facies; the mineralogical changes occurring in this well are comparable to those in well IID No. 2 (Figure 1 in Yau *et al.*, 1988) and Elmore 1 (Figure 2 in McDowell & Elders, 1980). XRD data revealed that kaolinite is abundant in sediments from the surface to a depth of ~300 m (T~115 °C); with increasing depth it decreases in abundance as the proportions of authigenic illite and chlorite increase; kaolinite is not observable at depths greater than ~500 m (T~160 °C). On the basis of previous XRD analyses, two samples were chosen for this study which bracket the sediment interval where the proportion of kaolinite decreases to the point where it is no longer detectable. These samples, chosen to be as separated by as small a sediment interval as possible given the set available, are composed of both cuttings and cores from depths of 256 and 477 m. According to the geothermal gradient for the SSGF, the corresponding temperatures are ~100 °C and ~200 °C, respectively (Sass *et al.*, 1988). These samples are referred to as "samples 256 and 477", below. XRD data on bulk samples showed that the principal minerals and their approximate relative proportions of both samples were identical, within error, to those determined by Cho *et al.* (1988) for the same well. McDowell & Elders (1980) and Yau *et al.* (1988) found similar mineralogical changes in Elmore 1 and IID 2 wells, respectively, verifying that they are representative of a well-defined sequence.

SEM observations using back-scattered electron (BSE) imaging were performed on both polished thin sections and ion-milled specimens using a HITACHI S-3200N SEM, equipped with a Noran X-ray energy-dispersive system (EDS), and operated at 20 kV. Following optical and BSE examination, a 3 mm aluminum washer was attached to the area of interest. The washer and sample (not expanded with L.R. White resin) were removed from the glass slide by melting the wax, and the sample was ion-milled, and carbon-coated. These procedures were designed to preserve original textures and to permit observation of (00l) lattice planes parallel to the electron beam. TEM observations and AEM (analytical electron microscopy) analyses were obtained with a Philips CM12 scanning-transmission electron microscope (STEM), operated at an accelerating voltage of 120 kV and beam current of ~10 μA. Lattice fringe images of phyllosilicates were obtained using 00l reflections at 75 000–100 000× magnification. Because beam damage is extremely rapid, through-focus series of images were not obtained. Initial focus was controlled manually by minimizing contrast, and images were taken at over-focus conditions (1000 Å) to optimize I-S contrast (Guthrie & Veblen, 1990). X-ray energy-dispersive spectra were obtained using a Kevex Quantum detector. A raster of 2000 × 2000 Å (as maximum size) in scanning mode was used to minimize alkali diffusion and volatilization. AEM quantitative chemical analyses were calculated from spectra using ion-milled standards of paragonite, muscovite, albite, clinochlore, fayalite, rhodonite, and titanite to derive k-ratios, following the procedure of Jiang *et al.* (1990).

Results

SEM observations

Figures 1a and 1b are back-scattered electron (BSE) micrographs of an ion-milled section of sample 256. Black areas are void spaces corresponding primarily to differential loss of fine-grained intergranular material during ion-milling, and in part due to original porosity. The grain-size distribution is distinctly bimodal, showing large (> 100 μm) detrital grains and a fine-grained matrix with grains < 1 μm in size. The matrix is comprised of a complex assemblage of detrital and authigenic minerals, most of which can only be identified by TEM (see below) because of their small sizes. Detrital minerals were identified primarily through EDS analyses, and consist mainly of quartz, plagioclase, biotite, muscovite, and kaolinite (Fig. 1a). Muscovite and biotite grains commonly show frayed ends with layer separation (Fig. 1b) apparently in response to deformation during burial; many consist of stacks of alternating packets of mica and kaolinite, but some grains are undeformed without any interlayered phase. The large quartz and plagioclase grains have rounded, irregular outlines (Fig. 1a, b), as clear evidence of corrosion through interaction with pore fluids. Void spaces have been partly cemented by sub- to euhedral crystals of auth-

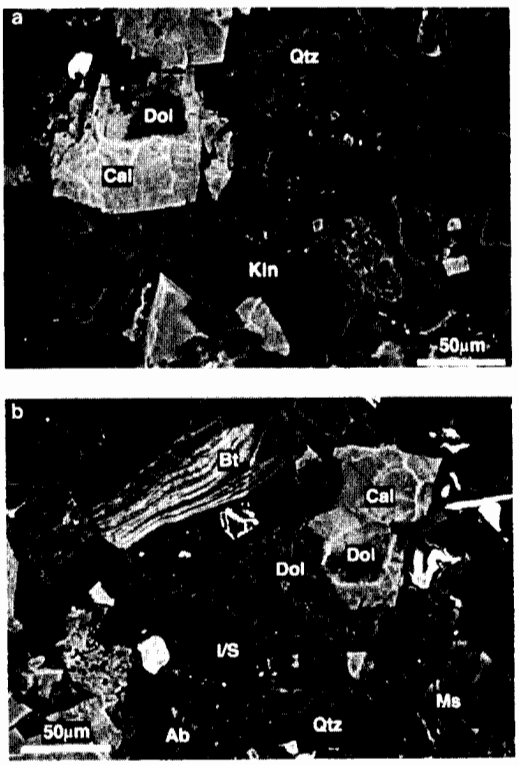

Fig. 1. BSE images of an ion-milled portion of sample 265. a) Large detrital grains of kaolinite (Kln) and quartz (Qtz) embedded in a fine-grained matrix; authigenic ferroan calcite (Cal) with dolomite cores (Dol); b) corroded quartz and albite (Ab) grains, altered muscovite (Ms), biotite (Bt) partly replaced by kaolinite, I/S in the fine-grained matrix.

igenic ferroan-calcite with dolomite cores. EDS analyses of the fine-grained matrix commonly correspond to a mixture of minerals, but are consistent with combinations of quartz, K-feldspar, calcite, illite, and I-S (I/S in Fig. 1b).

Kaolinite occurs in three distinctly different ways as imaged at the SEM scale: (1) As large detrital grains with sizes approaching 100 µm (Fig. 1a). Such grains have the same rounded, corroded appearance that characterizes feldspar and quartz grains. (2) As packets interlayered with layers of detrital biotite, forming biotite-kaolinite stacks (Fig. 1b). Muscovite occurs as muscovite - I-S stacks with similar appearances, but with no kaolinite detectable at the SEM scale. (3) In the fine-grained matrix, as implied by EDS analyes which are consistent with a mixture of kaolinite

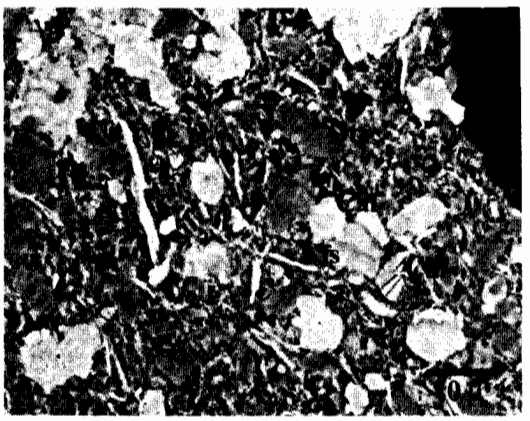

Fig. 2. BSE image of sample 477 showing typical sedimentary texture with a bimodal grain distribution involving large detrital grains and those in the matrix (as chlorite: Chl). Detrital, partly corroded quartz (Qtz) and K-feldspar (Kfs) grains are present. Calcite (Cal) occurs as a cement in open voids.

and I-S, and as verified by TEM observations (see below).

Figure 2 is a BSE image of an ion-milled washer of sample 477. The texture is still typical of a sediment with significant porosity. Large detrital grains are embedded in a fine-grained matrix. Detrital grains consist of quartz, K-feldspar, plagioclase, chlorite, and muscovite. No kaolinite was detected in the large detrital mica grains, nor was any implied by EDS analyses of the fine-grained matrix. As in sample 256, void spaces are cemented by authigenic calcite.

The principal minerals and their relative proportions as observed in thin sections and ion-milled samples by BSE imaging approximated those determined by bulk XRD data, as determined in this study and for the sequence as a whole. The ion-milled samples were therefore inferred to be representative of the sequence of mineral assemblages as determined by Cho *et al.* (1988). That is, they represent samples with significant detrital mica and kaolinite, and shallow kaolinite-free samples, respectively, as closely spaced as possible.

TEM - AEM observations

Sample 256. Rounded to sub-angular grains, largely of quartz, kaolinite, and muscovite, are embedded within finer-grained phyllosilicates

which are bent around the larger detrital grains (Fig. 3). Some open spaces are probably an artifact of ion-milling but many are typical of original pore space. Kaolinite is abundant, occurring as thick (0.25-μm thick) booklets (Fig. 4a) with boundaries typical of detrital grains. With the exception of local alteration to I-S described below, lattice-fringe images of kaolinite consist of well-defined, straight fringes with rare layer terminations. All selected-area diffraction patterns (SAED) give sharp reflections with no diffuseness (*e.g.*, Fig. 4b), non-00l reflections being consistent with well-ordered, one-layer polytypism. There is no indication of the two-layer polytypes dickite or nacrite.

I-S was observed by TEM in three modes of occurrence: as a partial replacement of kaolinite, as separate packets of layers within the fine-grained matrix, and as a partial replacement of detrital muscovite. Although the I-S stacking sequence varied locally, most consisted of (Reichweite) R1 I-S, which was identified in part by the typical alternating dark and light contrast of (001) fringes. The slightly wavy layers thus have 20-Å periodicity, the magnitude being in part due to dehydration of the smectite component in the vacuum of the TEM.

I-S occurs as thin packets of a few wavy layers between packets of unaltered kaolinite 300 to 1000 Å in thickness (Fig. 5). Unlike the textures observed in some other cases, as in alteration of muscovite to kaolinite (Jiang & Peacor, 1991), the interstratification of kaolinite packets occurs irregularly, therefore not giving rise to a superperiodicity in SAED patterns. In addition to packets internal to kaolinite grains, I-S also occurs as rims on 00l surfaces. The lattice-fringe contrast is often poorly defined in areas transitional from kaolinite to I-S; nevertheless, along-layer transitions from 7- to 10-Å fringes are commonly observed, as in Figure 5. Such features imply direct alteration of kaolinite layers to I-S, rather than the less-likely insertion of I-S between layers. SAED patterns of kaolinite with interstratified I-S packets retain the well-ordered peridiodicity, the

Fig. 3. Low-magnification (45000×) TEM image showing the typical texture of sample 265. Detrital quartz (Qtz) and kaolinite (Kln) grains are embedded in a fine-grained matrix of phyllosilicates.

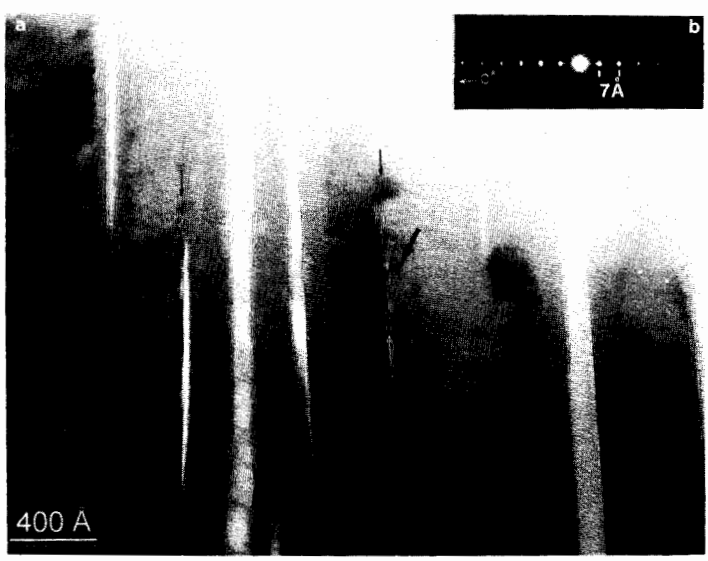

Fig. 4. a) Lattice-fringe image showing a thick kaolinite grain partially replaced by curved layers with 10 and 20-Å periodicities (thin arrows). The I-S layers separate 500 to 700-Å thick packets of straight, defect-free 7-Å layers. Thick arrow: enlarged area in Fig. 5. b) corresponding SAED pattern of kaolinite showing 00l reflections (sample 256).

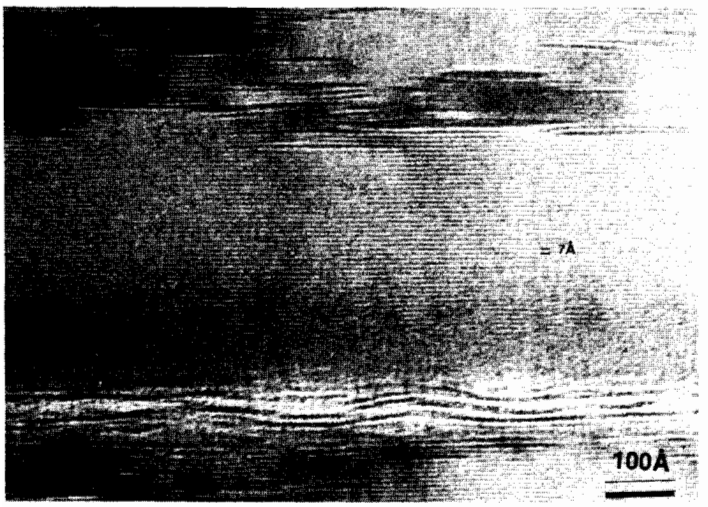

Fig. 5. Enlarged lattice-fringe image of Fig. 4a (thick arrow) showing curved I-S layers interlayered with kaolinite (straight 7-Å fringes); 10 and 20-Å periodicities are visible; thin arrow: along-layer transition from fringes with 7 to 10-Å spacings.

only change being the appearance of weak streaking along c*.

AEM analyses of pure kaolinite were easily obtained, but I-S packets are so thin that only analyses for which kaolinite was the dominant phase could be determined (Table 1). The resulting kaolinite formulae display a Si:Al ratio slightly greater than one, the deficiency in Al being compensated by Fe (most likely ferric iron). The analyses corresponding to kaolinite with I-S packets have small but significant Ca, K, Mg and Fe contents which are typical of inclusion of layers of dioctahedral I-S.

Figure 6a shows the textural relations typical of replacement of muscovite by I-S. Separate detrital grains of muscovite and kaolinite have subparallel 001 layers as shown by the TEM image and SAED pattern (Fig. 6b). I-S occurs as wavy, imperfect fringes along the 001 surfaces, those fringes apparently being continuous with the surface layers of muscovite and kaolinite. Along-layer transitions of muscovite to I-S occur. Diffuse, non-periodic reflections typical of I-S are superimposed on the sharp reflections of well-ordered muscovite, as consistent with parallel orientation of layers.

Figure 7 is a lattice-fringe image showing the textural relations typical of I-S occurring in the matrix. It shows up to 50-Å thick and 200-Å long flakes of slightly curved lattice fringes with 10 and 20-Å periodicites. Some of this material may be smectite rather than I-S, as the 20-Å periodicity typical of R1 I-S can be detected in such small grains only in some cases. These packets form aggregates with random orientation, filling void space. Interestingly, such packets, which appear to be as thin as two or three layers in some cases, are the thinnest ever detected in ion-milled samples in our laboratory. A small proportion approaches, but does not reach, the thinness required of fundamental particles.

Table 1. Representative AEM analyses of kaolinite (Kln) (1) and "altered" kaolinite (Kln+I-S) (2,3,4,5). All analyses have been normalized to 8 cations; all Fe assumed to be ferrous iron.

	1	2	3	4	5
Si	4.04	3.93	4.06	3.99	4.13
Al	3.87	4.03	3.94	3.97	3.79
Fe	0.09	0.04	–	0.04	0.09
Mg	–	0.09	0.19	0.15	0.14
Na	–	–	–	–	–
Ca	0.05	0.04	–	0.04	0.05
K	–	–	–	0.03	0.05
tot	8.05	8.13	8.19	8.22	8.24
Si/Al	1.04	0.98	1.03	1.01	1.09

I-S also occurs as packets several hundreds of angstroms in thickness, as shown in Figure 8a which is a lattice-fringe image showing I-S growing in contact with a detrital albite grain. Cross fringes are continuous through 4 to 5 layers with 20-Å periodicity, implying coherency across interlayers in I-S. The corresponding electron diffraction pattern (Fig. 8b) is typical of I-S, having 00l reflections that are broad and diffuse in a direction normal to c*, and non-00l reflections which are weak, diffuse, and non-periodic. Although such

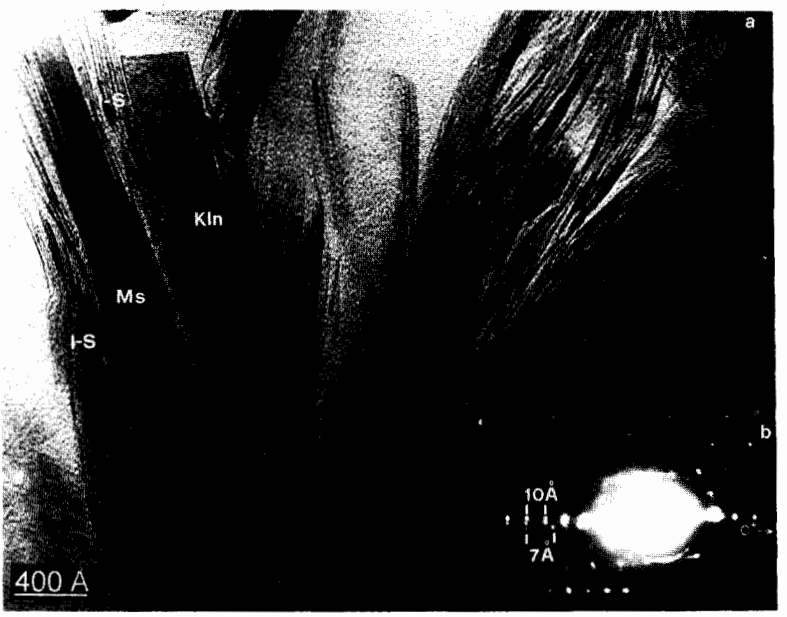

Fig. 6. a) Lattice-fringe image of muscovite (Ms) and kaolinite (Kln) in sample 256, replaced by I-S. b) Corresponding SAED pattern with 7 and 10-Å 001 reflections. Non-001 reflections are ill-defined, non-periodic, and diffuse, as typical of I-S.

extended sequences of I-S have a size consistent with detrital grains which have been entirely replaced, the general appearance is that of crystallization in pore space.

Sample 477. No kaolinite was detected in sample 477 by TEM imaging, as consistent with its absence as implied by both SEM and XRD data. By contrast, authigenic chlorite and illite are abundant, with lesser amounts of I-S. Representative textural features of sample 477 are shown in Figures 9–12.

Figures 9 and 10 show I-S typical of sample 477. In Figure 9, I-S occurs with layers subparallel to a crystal of quartz with apparent rhombohedral crystal faces. The terminal faces are inferred to be an overgrowth on a core (detrital ?) with irregular contrast, whereas the I-S appears to be neoformed in pore space. By contrast, thick I-S packets border a core of detrital muscovite, appearing to have an origin from layer-by-layer replacement. Figure 10 illustrates a detrital quartz grain with a shape reflecting dissolution rather

Fig. 7. Lattice-fringe image of small, curled I-S flakes neoformed in pore space; 10 and 20-Å fringes are present (sample 256).

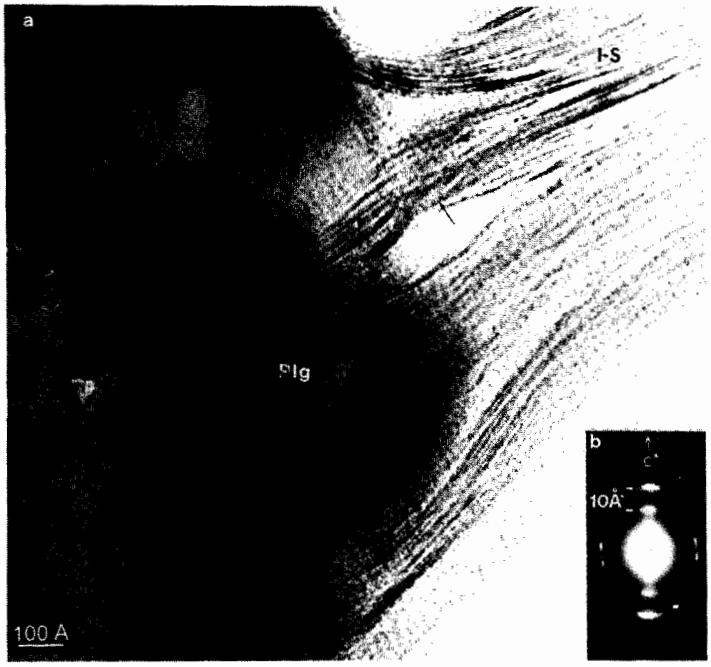

Fig. 8. a) Sample 256: Lattice-fringe image showing I-S adjacent to detrital plagioclase (Plg). Cross fringes (thin arrow) are continuous over 4 to 5 I-S layers. b) Corresponding SAED pattern with reflections with 10-Å spacing along c*; 00*l* reflections are broad and diffuse normal to c* and non-00*l* reflections are weak, diffuse, and non-periodic.

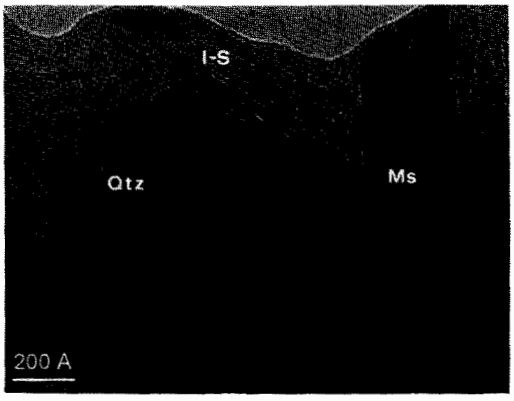

Fig. 9. TEM image of sample 477. I-S occurs rimming faces of a euhedral quartz (Qtz) crystal, having grown in pore space, and as a replacement of outer 001 layers of detrital muscovite (Ms).

than growth, with thin packets of I-S occupying void space and inferred to be neoformed.

Illite and chlorite are the most widespread authigenic minerals in sample 477, with a texture that is dramatically different from that of clay minerals in sample 256 (Fig. 11). Illite usually occurs in 100 to 200-Å thick packets characterized by high length/thickness ratio, uniform contrast, and constant 10-Å periodicity. The (001) layers are straight and comprise well-defined packets with sharp contacts. Packets may be slightly bent, and voids occur at low-angle grain boundaries. Authigenic chlorite similarly occurs as small packets up to 200-Å thick, commonly intergrown with illite packets. Those packets consist of 14-Å layers which are often bent and with layer terminations. Chlorite packets are always associated with illite packets (Fig. 11, 12), with low-angle grain boundaries (Fig. 11a) or parallel layers (Fig. 12a, b). Figure 12 shows a large, detrital muscovite grain (two-layer polytype, Fig. 12b) whose 001 planes are parallel to (001) of a smaller chlorite grain. Yau *et al.* (1987b) showed that samples, for which lattice-fringe images of ion-milled samples gave rise to sharply defined packets of illite and chlorite, gave images for separates which showed pseudohexagonal, euhedral crystals. Based on the similarily of their ion-milled images with those of sample 477, we infer that chlorite and illite with such euhedral shapes dominate the matrix of sample 477.

Discussion

Textural, chemical, and structural relations confirm that the transformation of kaolinite and the genesis of authigenic I-S and illite in the Salton Sea geothermal field are closely related, as im-

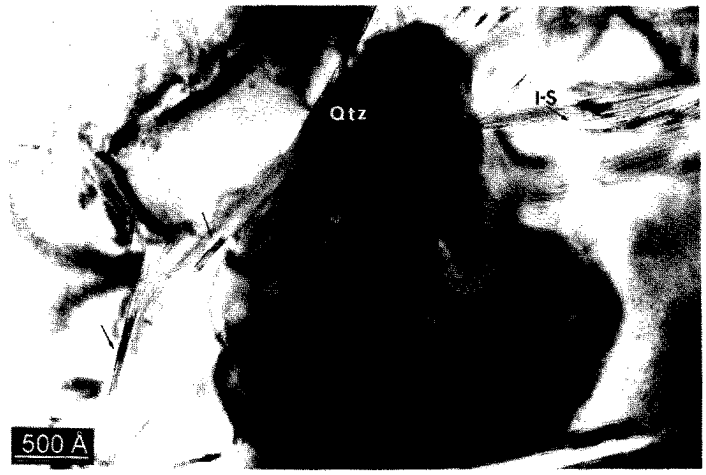

Fig. 10. TEM image of 477-m deep sample showing both detrital and authigenic phases. Neoformed small I-S packets occur in the matrix (thin arrows), near a corroded detrital quartz grain (Qtz).

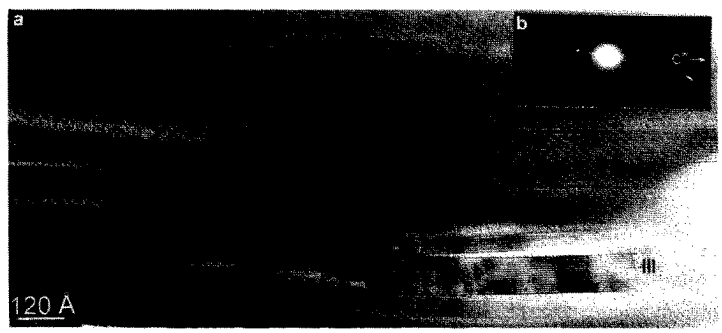

Fig. 11. a) Lattice-fringe image of sample 477 showing thin chlorite (Chl) and illite (Ill) packets with 14 and 10-Å periodicities, respectively. Packets are slightly bent, and low-angle grain boundaries are common. b) Corresponding SAED pattern of chlorite packets of differing orientations; 14-Å periodities are present along at least three different c* directions.

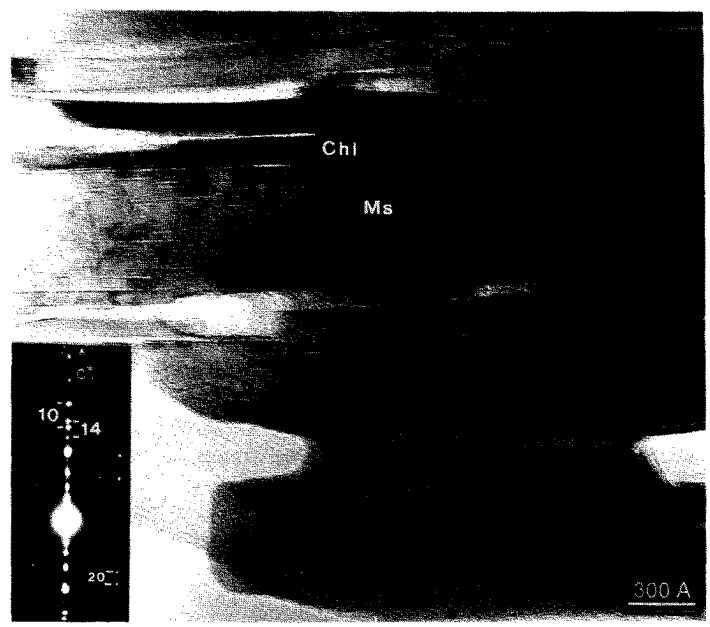

Fig. 12. a) Lattice-fringe image of sample 477 showing a detrital muscovite grain (Ms) bordered by a packet of authigenic chlorite (Chl) with slightly bent 001 planes. b) Corresponding SAED pattern with 10 and 14-Å reflections along c*; non-001 reflections have 20-Å periodicity typical of muscovite $2M_1$.

plied by XRD data. They result from interaction with hydrothermal fluids and are characterized by dissolution and crystallization, but with the scale of reaction varying from the atomic scale of individual layers to large-scale transport of reaction components in the same samples.

BSE images of sample 256 show that it contains abundant kaolinite as large anhedral, detrital grains, and as a component of biotite-kaolinite and muscovite-kaolinite stacks. Muscovite is common as large detrital grains. TEM observations show that the fine-grained matrix also contains abundant detrital muscovite and kaolinite grains. Detrital material thus occurs in two very different and largely separate grain-size distributions. Biotite-kaolinite stacks have a detrital texture as well, suggesting that they formed during weathering or hydrothermal alteration of the source-rock, rather than having kaolinite introduced as an authigenic component.

The collective data show that both detrital kaolinite and muscovite are progressively replaced by I-S in the first 500 m of the sedimentary sequence. This reaction goes to completion at 200 °C. Indeed, in samples from depths deeper than 400 m, which corresponds to temperatures >200 °C, kaolinite is absent whereas I-S, illite and chlorite are abundant. I-S forms by two separate mechanisms: (1) by direct replacement of layers of muscovite or kaolinite, referred to as an "along-layer transition", and (2) by direct precipitation in pore space, separate from detrital grains but intimately associated with them; *i.e.*, by crystallization. Subsequently, the I-S content diminishes as shown by XRD data, and detrital kaolinite and (at greater depths) muscovite are no longer detectable, having been replaced by euhedral packets of illite and chlorite.

Along-layer transitions such as that from kaolinite (001) to I-S might be considered to be a solid-state transformation such as proposed by Altschuler *et al.* (1963). Such a transformation involves major changes in structure, however, with the addition of and/or reversal in orientation of tetrahedral sheets. Significant chemical changes occur as Si is replaced by Al in tetrahedral sheets and Mg and Fe enter the octahedral sheet; interlayer cations (K^+, Na^+, Ca^{2+}) are added to the structure. These drastic changes occur at low temperatures where diffusion rates are minimal. These relations imply that the kaolinite structure is locally disarticulated and reconstituted as I-S. That is, the process is one of local dissolution and crystallization. The same relations are applicable to the process of replacement of muscovite by I-S. TEM studies have documented that layer-by-layer transitions (*e.g.*, Ahn & Peacor, 1986, 1987; Giorgetti *et al.*, 1997) occur by local dissolution and crystallization in many cases. It is now generally accepted that such relations are universal and that solid-state reactions are at best unlikely.

The neocrystallization of I-S in pore space, separate from detrital grains, must also be a process involving dissolution of detrital muscovite and kaolinite. The chemical components derived from such dissolution must be transported over distances at least on the order of the dimensions of pore space, however, resulting in crystallization of separate packets. The mechanisms of layer-by-layer replacement and crystallization are effectively the same, differing only in the scale of transport of reactants. This is analogous to mechanisms of transformation of smectite to illite in closed as opposed to open systems (*e.g.*, Yau *et al.*, 1987 b).

The observed features are consistent with the assumption that the alteration process occurs through a series of irreversible reactions between interstitial fluids and detrital minerals. These reactions are strongly controlled by the pH value and the activity of K^+ in the fluid. Both kaolinite and muscovite are no longer stable in the presence of a Na^+, Ca^{2+}, K^+-rich brines with a relatively low pH. Muscovite reacts to I-S; on the other hand, kaolinite reacts to I-S without forming pyrophyllite, implying that the reaction

kaolinite + quartz + fluid = I-S + fluid

has occurred. As emphasized by Essene & Peacor (1995), the collective data indicate that all detrital phases and I-S are metastable and that the series of dissolution-recrystallization reactions which characterizes the open fluid-rock system of the Salton Sea Geothermal Field represent steps in an Ostwald step sequence toward a stable system which includes chlorite and muscovite.

At greater depths, kaolinite is not detectable. Chlorite and illite, with some remnants of I-S, represent the newly-formed authigenic phyllosilicates. Clearly Mg^{2+}, Fe^{2+}, Al^{3+}, Si^{4+}, and K^+ derived from dissolution of detrital K-feldspar, muscovite, and biotite, participate in the crystallization of the authigenic mineral assemblage, and in particular to formation of I-S, whether by along-layer transformation or crystallization. All data are consistent with transformation mechan-

isms in the Salton Sea sequence that involve dissolution of original phases, transportation of dissolved species by the geothermal brines, and crystallization from solution.

Origin of stacks

Phyllosilicate stacks consist of alternating packets of two different phyllosilicates, commonly chlorite and muscovite. Their origin has been the subject of intensive study, indicating that they have formed or have been modified during a pre-sedimentation event, authigenesis, or stress during metamorphism (see Li *et al.*, 1994 and references therein for review). The conclusions of some studies are problematic in that high-resolution data on textures and compositions have been lacking, but recent studies (Li *et al.*, 1994, 1998; Jiang *et al.*, 1990) have documented the origin of muscovite-chlorite stacks from a detrital precursor which could be either muscovite or biotite, as modified during low-grade metamorphism. A pre-sedimentary origin is perhaps the least-verified.

The muscovite-kaolinite and biotite-muscovite stacks observed in sample 265 have overall sizes and shapes that imply a detrital origin. In other studies, stacks have been observed to form by addition of a second clay mineral along 001 cleavages opened by strain, with subparallel layers of the added mineral commonly terminating against bounding layers of the strained, original mineral. The material of this study, however, shows none of the strain features typical of such relations. Kaolinite and micas have cross-cutting surfaces consistent with both minerals having preceded formation of such erosional features. By contrast, other studies have documented how along-layer transitions can result in alternating packets. For example, Ahn & Peacor (1987) and Jiang & Peacor (1991) showed how packets of biotite and kaolinite, and muscovite and kaolinite, respectively, could be formed by along-layer transformation of primary mica during regional hydrothermal alteration, but those materials had not been subjected to erosion and sedimentation. We infer that the stacks in shallow Salton Sea-area sediments are the equivalent of such materials, and have a pre-sedimentation origin. Such an origin for kaolinite in stacks is also implied by the presence of kaolinite in the process of altering in the same samples. It is unlikely that chemical conditions in such an open system would vary so radically over short distances as to result in kaolinite appearing as a reactant and product in separate, adjacent reactions.

Our observations do not include modification of the stacks at greater depths. However, it is well known that biotite is commonly replaced by corrensite and then chlorite during diagenesis. Likewise, I-S commonly transforms to illite and then illite to muscovite. We hypothesize therefore, that some biotite-kaolinite stacks have a pre-sedimentation origin and that subsequent prograde reactions could well result in formation of chlorite-muscovite stacks. It thus appears that such stacks can form by a great variety of mechanisms, and that the processes reviewed by Li *et al.* (1994) is at least in part an expression of that variety, rather than misinterpretation of only one universal mechanism.

Acknowledgments: We are grateful to C. Henderson and L.-S. Kao for help with the experimental parts of this project. We also acknowledge M. Tribaudino and A. Gualtieri for their constructive reviews. This research was supported by NSF grant EAR-9418108.

References

Ahn, J.H. & Peacor, D.R. (1985): Transmission electron microscopy study of diagenetic chlorite in Gulf Coast argillaceous sediments. *Clays Clay Min.*, **33**, 228-236.

– – (1986): Transmission and analytical electron microscopy of the smectite-to-illite transition. *Clays Clay Min.*, **34**, 165-179.

– – (1987): Kaolinitization of biotite: TEM data and implications for an alteration mechanism. *Am. Mineral.*, **72**, 353-356.

Altschuler, Z.S., Dwornik, E.J., Kramer, H. (1963): Transformation of montmorillonite to kaolinite during weathering. *Science*, **141**, 148-152.

Arostegui, J., Zuluaga, M.C., Velasco, F., Ortega-Huertas, M., Nieto, F. (1991): Diagenesis of the central Basque-Cantabrian Basin (Iberian Peninsula) based on illite-smectite distribution. *Clay Min.*, **26**, 535-548.

Boles, J.R. & Franks, S.G. (1979): Clay diagenesis in Wilcox sandstones of southwest Texas: Implications of smectite diagenesis on sandstone cementation. *J. Sediment. Petrol.*, **49**, 55-70.

Cho, M., Liou, J.G., Bird, D.K. (1988): Prograde phase relations in the State 2-14 well metasandstones, Salton Sea Geothermal Field, California. *J. Geophys. Res.*, **93**, 13081-13103.

Essene, E. J. & Peacor, D. R. (1995): Clay mineral thermometry – a critical perspective. *Clays Clay Min.*, **43**, 540-553.

Frey, M. (1987): Low-temperature metamorphism. Blackie & Son, eds., Glasgow, 351 p.

Giorgetti, G., Memmi, I., Nieto, F. (1997): Microstructures of intergrown phyllosilicate grains from Verrucano metasediments (northern Apennines, Italy). *Contrib. Mineral. Petrol.*, **128**, 127-138.

Guthrie, G.D., Jr. & Veblen, D.R. (1990): Interpreting one-dimensional high-resolution transmission electron micrographs of sheet silicates by computer simulation. *Am. Mineral.*, **75**, 276-288.

Helgeson, H. C. (1967): Solution chemistry and metamorphism. *in* "Researches in Geochemistry, v. II", P.H. Abelson ed., John Wiley and Sons, New York, 362-404.

– (1968): Geological and thermodynamic characteristics of the Salton Sea Geothermal System. *Am. J. Sci.*, **266**, 129-166.

Hower, J., Eslinger, E.V., Hower, M.E., Perry, E.A. (1976): Mechanism of burial metamorphism of argillaceous sediments: 1. Mineralogical and chemical evidence. *Geol. Soc. Am. Bull.*, **87**, 725-737.

Jiang, W.T. & Peacor, D.R. (1991): Transmission electron microscopic study of the kaolinitization of muscovite. *Clays Clay Min.*, **39**, 1-13.

Jiang, W.T., Peacor, D.R., Merriman, R.J., Roberts, B. (1990): Transmission and analytical electron microscopic study of mixed-layer illite/smectite formed as an apparent replacement product of diagenetic illite. *Clays Clay Min.*, **38**, 449-468.

Li, G., Peacor, D., Essene, E. J. (1998): The formation of sulfides during alteration of biotite to chlorite-corrensite. *Clays Clay Min.*, **46**, 649-657.

Li, G., Peacor, D.R., Merriman, R.J., Roberts, B., van der Pluijm, B.E. (1994): TEM and AEM constraints on the origin and significance of chlorite-mica stacks in slates: an example from Central Wales, U.K. *J. Struct. Geol.*, **16**, 1139-1157.

McDowell, S.D. (1986): Composition and structural state of coexisting feldspars, Salton Sea geothermal field. *Min. Mag.*, **50**, 75-84.

McDowell, S.D. & Elders, W.A. (1980): Authigenic layer silicate minerals in borehole Elmore 1, Salton Sea Geothermal Field, California, USA. *Contrib. Mineral. Petrol.*, **74**, 293-310.

McDowell, S.D. & Paces, J.B. (1985): Carbonate alteration minerals in the Salton Sea geothermal system, California, USA. *Min. Mag.*, **49**, 469-479.

Merriam, R. & Bandy, O.L. (1965): Source of upper Cenozoic sediments in the Colorado delta region. *J. Sediment. Petrol.*, **35**, 911-916.

Muffler, L.P.J. & Doe, B.R. (1968): Composition and mean age of detritus of the Colorado River delta in the Salton Trough, southeastern California. *J. Sediment Petrol.*, **38**, 384-399.

Muffler, L.P.J. & White, D.E. (1969): Active metamorphism of Upper Cenozoic sedments in the Salton Sea Geothermal Field and the Salton trough, southeastern California. *Geol. Soc. Am. Bull.*, **80**, 157-182.

Nieto, F., Ortega-Huertas, M., Peacor, D.R., Arostegui, J. (1996): Evolution of illite/smectite from early diagenesis through incipient metamorphism in sediments of the Basque-Cantabrian Basin. *Clays Clay Min.*, **44**, 304-323.

Primmer, T.J. (1985): A transition from diagenesis to greenschist facies within a major Variscan fold/thrust complex in south-west England. *Min. Mag.*, **49**, 365-374.

Ruiz-Cruz, M.D. & Andreo, B. (1996): Genesis and transformation of dickite in Permo-Triassic sediments (Betic Cordilleras, Spain). *Clay Min.*, **31**, 133-152.

Sass, J.H., Priest, S.S., Duda, L.E., Carson, C.C., Hendricks, J.D., Robison, L.C. (1988): Thermal regime of the state 2-14 well, Salton Sea Scientific Drilling Project. *J. Geophys. Res.*, **93**, 12995-13004.

Shearer, C.K., Papike, J.J., Simon, S.B., Davis, B.L. (1988): Mineral reactions in altered sediments from the California State 2-14 well: Variation in the modal mineralogy, mineral chemistry and bulk composition of the Salton Sea scientific drilling project core. *J. Geophys. Res.*, **93**, 104-122.

Yau, Y.C., Peacor, D.R., Beane, R.E., Essene, E.J., McDowell, S.D. (1988): Microstructures, formation mechanism, and depth-zoning of phyllosilicates in geothermally altered shales, Salton Sea, California. *Clays Clay Min.*, **36**, 1-10.

Yau, Y.C., Peacor, D.R., Essene, E.J. (1987a): Authigenic anatase and titanite in shales from the Salton Sea Geothermal Field, California. *N. Jahrb. Mineral., Mh.*, **1987**, 441-452.

Yau, Y.C., Peacor, D.R., McDowell, S.D. (1987b): Smectite-to-illite reactions in Salton Sea shales: A transmission and analytical electron microscopy study. *J. Sediment. Petrol.*, **57**, 335-342.

Younker, L.W., Kasameyer, P.W., Tewhey, J.D. (1982) Geological, geophysical, and thermal characteristics of the Salton Sea geothermal field, California. *J. Volcanol. Geoth. Res.*, **12**, 221-258.

Received October 1999
Modified version received 6 March 2000
Accepted 27 March 2000